nature photonics

SUPPLEMENTARY INFORMATION

https://doi.org/10.1038/s41566-018-0269-2

In the format provided by the authors and unedited.

Thermal-motion-induced non-reciprocal quantum optical system

Shicheng Zhang[1], Yiqi Hu[1], Gongwei Lin[1]*, Yueping Niu[1]*, Keyu Xia[2,3]*, Jiangbin Gong[4] and Shangqing Gong[1]

[1]Department of Physics, East China University of Science and Technology, Shanghai, China. [2]National Laboratory of Solid State Microstructures, College of Engineering and Applied Sciences, and School of Physics, Nanjing University, Nanjing, China. [3]Collaborative Innovation Center of Advanced Microstructures, Nanjing University, Nanjing, China. [4]Department of Physics, National University of Singapore, Singapore, Singapore. *e-mail: gwlin@ecust.edu.cn; niuyp@ecust.edu.cn; keyu.xia@nju.edu.cn

Supplementary Information: Thermal-motion-induced non-reciprocal quantum optical system

Shicheng Zhang[1], Yiqi Hu[1], Gongwei Lin[1],* Yueping Niu[1],† Keyu Xia[2,3],‡ Jiangbin Gong[4], and Shangqing Gong[1]
[1] *Department of Physics, East China University of Science and Technology, Shanghai 200237, China.*
[2] *National Laboratory of Solid State Microstructures, College of Engineering and Applied Sciences, Nanjing University, Nanjing 210008, China.*
[3] *Collaborative Innovation Centre of Advanced Microstructures, Nanjing 210093, China and*
[4] *Department of Physics, National University of Singapore, 117542, Singapore.*

This supplementary information provides (i) theoretical understanding of the demonstrated optical non-reciprocity, (ii) other details about our experimental implementation and (iii) some additional experiment results.

I. THEORETICAL MODEL

In this section, we will describe a theoretical model for realizing non-reciprocal transmission. Our experiment is guided by our theoretical insights and the experimental results agree with the theory below.

A. The atom-cavity system

As discussed in the main manuscript, the cavity quantum electrodynamic (cQED) system involves a three-mirror ring cavity coupled to an ensemble of Λ-type atoms undergoing thermal motion. The atom has one excited state $|3\rangle$, and two ground states $|1\rangle$ and $|2\rangle$. The cavity mode has a resonance frequency of ω_a, and is coupled to the atomic transition of $|1\rangle \leftrightarrow |3\rangle$ with a single-photon rate g. Because the number of atoms N is large, we can replace the rate for each atom with the average value. The atomic transition of $|2\rangle \leftrightarrow |3\rangle$ is driven by a strong control laser beam with a carrier frequency ω_c and a Rabi frequency Ω_c. The probe field with frequency ω_p is injected into the ring cavity at a rate κ_1 through the mirror M1 and exits from the mirror M3 at a rate of κ_2 (see Fig. S3 for our experimental setup).

The Hamiltonian describing the motion of the cQED system, including the input, takes the following form ($\hbar = 1$):

$$\begin{aligned} H =& \omega_a \hat{a}^\dagger \hat{a} + \sum_{j=1}^{N} \left[\sum_{l=1}^{3} \omega_l \hat{\sigma}_{ll}^{(j)} + \Omega_c \left(e^{-i\omega_c t} \hat{\sigma}_{32}^{(j)} + e^{i\omega_c t} \hat{\sigma}_{23}^{(j)} \right) + g \left(\hat{a}^\dagger \hat{\sigma}_{13}^{(j)} + \hat{a} \hat{\sigma}_{31}^{(j)} \right) \right] \\ &+ i\sqrt{\kappa_1} \left(e^{-i\omega_p t} \hat{a}^\dagger \hat{a}_p - e^{i\omega_p t} \hat{a}_p^\dagger \hat{a} \right) , \end{aligned} \tag{S1}$$

where ω_l $(l = 1, 2, 3)$ is the energy of state $|l\rangle$; $\sigma_{lm}^{(j)} = |l\rangle_j \langle m|$ $(l, m = 1, 2, 3)$ is the atomic operator of the jth atom, $\hat{a}$ ($\hat{a}^\dagger$) is the annihilation (creation) operator of the cavity mode, $\hat{a}_p$ ($\hat{a}_p^\dagger$) is the annihilation (creation) operator of the probe field.

In the rotating frame defined by the unitary transformation

$$U = \exp \left\{ -i\omega_p \hat{a}^\dagger \hat{a} t - i \sum_{j=1}^{N} \left[(\omega_3 - \omega_p) \sigma_{11}^{(j)} + (\omega_3 - \omega_c) \sigma_{22}^{(j)} + \omega_3 \sigma_{33}^{(j)} \right] t \right\} , \tag{S2}$$

we have

$$H' = \Delta_p \hat{a}^\dagger \hat{a} - \sum_{j=1}^{N} \left[\Delta_p \hat{\sigma}_{11}^{(j)} + \Delta_c \hat{\sigma}_{22}^{(j)} \right] + \sum_{j}^{N} \left[\Omega_c \left(\hat{\sigma}_{32}^{(j)} + \hat{\sigma}_{23}^{(j)} \right) + g \left(\hat{a}^\dagger \hat{\sigma}_{13}^{(j)} + \hat{a} \hat{\sigma}_{31}^{(j)} \right) \right] + i\sqrt{\kappa_1} \left(\hat{a}^\dagger \hat{a}_p - \hat{a}_p^\dagger \hat{a} \right) , \tag{S3}$$

*Electronic address: gwlin@ecust.edu.cn
†Electronic address: niuyp@ecust.edu.cn
‡Electronic address: keyu.xia@nju.edu.cn

where $\Delta_a = \omega_a - \omega_p$, $\Delta_p = \omega_3 - \omega_1 - \omega_p$ and $\Delta_c = \omega_3 - \omega_2 - \omega_c$. This Hamiltonian is obtained in the absence of any thermal motion of the atoms. However, in our actual system each atom moves randomly due to their thermal energy. Such inevitable thermal motion causes random Doppler shifts at the microscopic level. Below, we take into account this microscopic Doppler effect.

B. Quantum Langevin equations with microscopic Doppler shifts

Random thermal motion is inevitable for atoms. When atoms interact with photons, the frequencies of photons "seen" by the atoms can be modified by the thermal motion due to the induced microscopic Doppler shift. This is more for atoms at room temperature. The resulting Doppler shifts are random for each atom because its motion is random, with the velocity satisfying the Maxwell-Boltzmann distribution. For this reason, thermal motion is typically considered as a detrimental effect and thus should be avoided in quantum coherent control of photons with atoms. This takes us to the traditional concept that cold atoms are much more useful than hot atoms because the effect of thermal motion in the former is much smaller than the latter.

However, counter-intuitively, in this work we make use of the thermal motion of warm atoms as a useful resource to create a non-reciprocal quantum optical system. Our scheme involves the creation of intracavity electromagnetically induced transparency (EIT) with a strong control field. In combination with the unidirectionality of the control laser beam, the microscopic Doppler shifts can cause a *chiral susceptibility* depending on the propagation direction of the probe field. In the regime of collectively strong coupling between the atoms and the cavity, a probe field entering this chiral cQED system displays transmission features critically dependent on its propagation direction, generating non-reciprocal optics.

Note that thermal motion is completely random and isotropic, as schematically shown in Fig. 1c in the main manuscript. If we decompose the velocity of atoms into three orthogonal components in the Cartesian coordinate system, then the number density distribution of velocity in each component is the same. But for warm Rubidium (Rb) atoms at room temperature with a velocity v ($|v|/c \ll 1$, c is the velocity of light), we only need considering the longitudinal Doppler effect $\Delta\omega_{\parallel} = \omega v_{\parallel}/c$ (the transverse Doppler effect $\Delta\omega_{\perp} = \omega(v_{\perp}/c)^2$ can be ignored), here $v_{\parallel}$ and $v_{\perp}$ are the longitudinal and transvere velocity components parallel and perpendicular to the propagation direction of laser beams, respectively [1]. So, we will neglect the small transverse Doppler shift in taking into account the detunings between lasers and the atomic transitions below. The integral of the number density distribution over the transverse velocity components yields unity and thus has no effect on the susceptibility. To include the effect of thermal motion in our theory, we only need to consider the velocity component along the laser beam. For simplicity, we remove the subscript $\parallel$ in the longitudinal velocity component. For jth atom moves with an individual velocity v_j along the laser beam, its motion causes an additional detuning proportional to v_j, known as the microscopic Doppler shift. Accordingly, we need to replace Δ_a and Δ_c with $\Delta_a + k_a v_j$ and $\Delta_c + k_c v_j$, where k_a and k_c are the wave vectors of the cavity mode and the control field. To a good approximation, we can assume that the wave vectors of all involved fields have the same amplitude, $|k_a| = |k_c| = |k|$. Dependent on the propagation direction of field, the atom reacts to the driving field with an additional detuning kv_j. k takes the "+" ("-") sign when the jth atom moves towards (away from) the field [2]. When the probe field and the control field propagate along the same direction, they "see" the same Doppler shift, $k_a = k_c$. By contrast, the Doppler shifts are opposite in the counter-propagation case, $k_a = -k_c$. Due to this microscopic Doppler effect manifesting differently for co-propagating and counter-propagating cases and given the unidirectional propagation direction of the control laser beam, the intracavity EIT becomes chiral for the probe field. After taking into account the thermal-motion-induced Doppler shifts, the quantum Langevin equations describing the motion of this chiral cQED system takes the following form: [3]

$$\dot{\hat{a}} = -(i\Delta_a + \frac{\kappa}{2})\hat{a} - ig\sum_{j=1}^{N}\sigma_{13}^{(j)} + \sqrt{\kappa_1}\hat{a}_p \,, \tag{S4}$$

$$\dot{\hat{\sigma}}_{13}^{(j)} = -i(\Delta_a + \Delta_p + k_a v_j)\hat{\sigma}_{13}^{(j)} - \gamma_3\hat{\sigma}_{13}^{(j)} - i\Omega_c\hat{\sigma}_{12}^{(j)} + ig(\hat{\sigma}_{33}^{(j)} - \hat{\sigma}_{11}^{(j)})\hat{a} \,, \tag{S5}$$

$$\dot{\hat{\sigma}}_{12}^{(j)} = -i\left[(\Delta_a + \Delta_p + k_a v_j) - (\Delta_c + k_c v_j)\right]\hat{\sigma}_{12}^{(j)} - \gamma_{12}\hat{\sigma}_{12}^{(j)} - i\Omega_c\hat{\sigma}_{13}^{(j)} + ig\hat{\sigma}_{32}^{(j)}\hat{a} \,, \tag{S6}$$

where $\kappa = \kappa_1 + \kappa_2 + \kappa_c$, κ_c is the cavity intrinsic damping rate, γ_3 is the spontaneous decay rate associated with the state $|3\rangle$ and γ_{12} is the dephasing rate between the two ground states of $|1\rangle$ and $|2\rangle$.

C. Transmission in the steady state

We are interested in the transmission spectrum which can be obtained in the steady state by setting $\langle\dot{\hat{a}}\rangle = 0$, $\langle\dot{\hat{\sigma}}_{13}^{(j)}\rangle = 0$, and $\langle\dot{\hat{\sigma}}_{12}^{(j)}\rangle = 0$. In our configuration with $|g| \ll \Omega_c$, we have $\langle\hat{\sigma}_{11}^{(j)}\rangle \approx 1$ and $\langle\hat{\sigma}_{32}^{(j)}\rangle \approx 0$. Solving the steady-state solution and converting the sum of velocities into an integral, we arrive at

$$\hat{a} = \frac{\sqrt{\kappa_1}\hat{a}_p}{i\Delta_p + \kappa/2 + i\chi} , \tag{S7}$$

$$\chi = \int_{-\infty}^{\infty} \frac{-iN|g|^2 D(v)}{\gamma_3 + i(\Delta_a + \Delta_p + k_a v) + \frac{|\Omega_c|^2}{\gamma_{12} + i[(\Delta_a - \Delta_c + \Delta_p) + (k_a v - k_c v)]}} dv , \tag{S8}$$

where $D(v) = e^{-v^2/v_p^2}/(v_p\sqrt{\pi})$ is the Maxwell-Boltzmann velocity distribution of atoms and $v_p = \sqrt{2k_BT/m}$ is the most probable velocity. k_B is the Boltzmann constant, T is the absolute temperature and m is the atomic mass. χ is the overall susceptibility of the ensemble of atoms to the cavity mode. When the cavity mode and the control field co-propagate along the same direction, we have $k_a = k_c = k$. Otherwise, $k_a = -k_c = k$ when they counter-propagate. The output transmission from Mirror 3 is $\hat{a}_{\text{out}} = \sqrt{\kappa_2}\hat{a}$.

In our experiment, we choose $\Delta_c = \Delta_a = 0$. Thus, the transmission amplitude for the co-propagation case and the counter-propagation case is given by [4]

$$t_{\text{co(cou)}}(\Delta_p) = \frac{\sqrt{\kappa_1\kappa_2}}{i\Delta_p + \frac{\kappa}{2} + i\chi_{\text{co(cou)}}} , \tag{S9}$$

with

$$\chi_{\text{co}} = \int_{-\infty}^{\infty} \frac{-iN|g|^2 D(v)}{\gamma_3 + i(\Delta_p + kv) + \frac{\Omega_c^2}{\gamma_{12} + i\Delta_p}} dv , \tag{S10}$$

and

$$\chi_{\text{cou}} = \int_{-\infty}^{\infty} \frac{-iN|g|^2 D(v)}{\gamma_3 + i(\Delta_p + kv) + \frac{\Omega_c^2}{\gamma_{12} + i(\Delta_p + 2kv)}} dv . \tag{S11}$$

The transmission spectra for these two cases in the steady state are given by

$$T_{\text{co(cou)}} = |t_{\text{co(cou)}}(\Delta_p)|^2 = \left| \frac{\sqrt{\kappa_1\kappa_2}}{i\Delta_p + \frac{\kappa}{2} + i\chi_{\text{co(cou)}}} \right|^2 . \tag{S12}$$

Clearly, according to Eq. S12, the probe field transmission can be very different, i.e. non-reciprocal in these two cases if the chiral susceptibility is large enough, which is true if the collective coupling strength $\sqrt{N}g$ is large enough. In addition, from the theory above we can see that in terms of probe field transmission, reversing the control laser beam is equivalent to reversing the probe field.

In the main manuscript, we have shown the transmission as a function of the control field strength and collective coupling strength. Here, we choose three typical values of collective coupling strength: $\sqrt{N}g = 0.1\kappa$, $\sqrt{N}g = \kappa$ and $\sqrt{N}g = 10\kappa$, to show the dependence of co- and counter-propagation transmissions on the control field strength and collective coupling strength, see Fig. S1. When the collective coupling strength is small, both co- and counter-propagation cases yield high transmission, thus it is hard to see the ONR. In the CSCR, e.g. $\sqrt{N}g = 10\kappa$, the co-propagation transmission can approach to unity when Ω_c is large enough, whereas the counter-propagation transmission remains very low. Therefore, a strong ONR is a result of the combined effects of the susceptibility-momentum locking-induced chirality and the large VRS in the CSCR.

D. Doppler effect of transmission contrast

In order to evaluate the Doppler effect on the non-reciprocity, we theoretically calculate the transmission contrast versus temperature under the same collectively strong coupling condition (that is, without accounting for the possible change in the number of the atoms in the cavity). It is seen from Fig. S2 that, in the room temperature range, the system exhibits strong non-reciprocity and the obtained non-reciprocity remains unchanged with the change in the

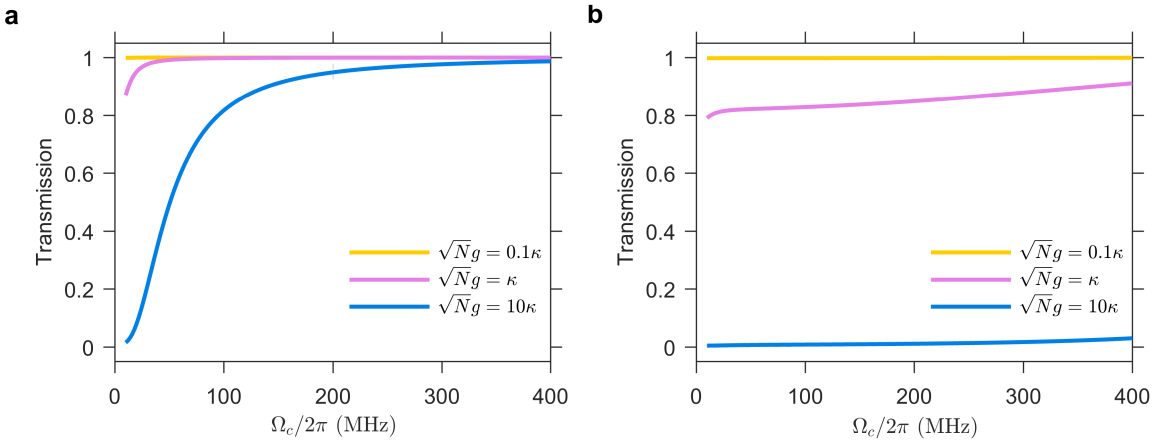

FIG. S1: **Non-reciprocal transmission vs the control field strength with different collective coupling strength.** The co-propagating transmission (**a**) and the counter-propagating transmission (**b**) as a function of the control field strength with $\sqrt{N}g = 0.1\kappa, 1\kappa, 10\kappa$. The parameters are $\Delta_c = \Delta_p = 0$ MHz, $\{\kappa_1/2\pi, \kappa_2/2\pi, \kappa_c/2\pi\} = \{0.5, 4, 6\}$ MHz, $\Gamma_3/2\pi = 10$ MHz, $\gamma_{12}/2\pi = 0.8$ MHz, $\lambda = 2\pi/k = 795$ nm and $T = 55$ °C.

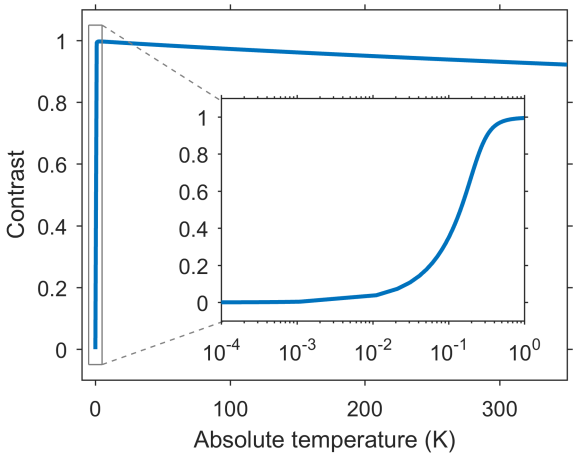

FIG. S2: **Transmission contrast as a function of temperature.** Parameters are $\sqrt{N}g = 2\pi \times 80$ MHz, $\Omega_c = 2\pi \times 30$ MHz and $\kappa = 2\pi \times 10$ MHz, which are based on our experimental condition.

temperature. From the inset of Fig. S2, one also sees that only when the temperature is below mK, will the system exhibit clear reciprocity, that is, showing the absence of non-reciprocal effects due to the negligible role of thermal motion of the atoms.

II. EXPERIMENTAL SETUP

A. Detailed experimental setup for warm atoms

Figure S3 shows a detailed schematic of the experimental setup for the demonstration of thermal-motion-induced ONR. In our experiment, the ring cavity composes of a flat mirror M3 with reflectivity of 99 % and two concave mirrors M1 and M2 (curvature radius 40 cm) with reflectivity of 99.95 %. The cavity mirror M2 is mounted on a piezoelectric transducer (PZT) for cavity frequency detuning. The optical path length of the cavity is about 49 cm, corresponding to a free spectral range (FSR) about 600 MHz. The fineness of the empty cavity (without the Rb vapor cell and PBSs) is about 300. After inserting the Rb vapor cell and cubic polarization beam splitters (PBS1,2), the fineness of the cavity reduces to 60, which corresponds to a cavity decay rate about 10 MHz. The Rb vapor cell is 5 cm

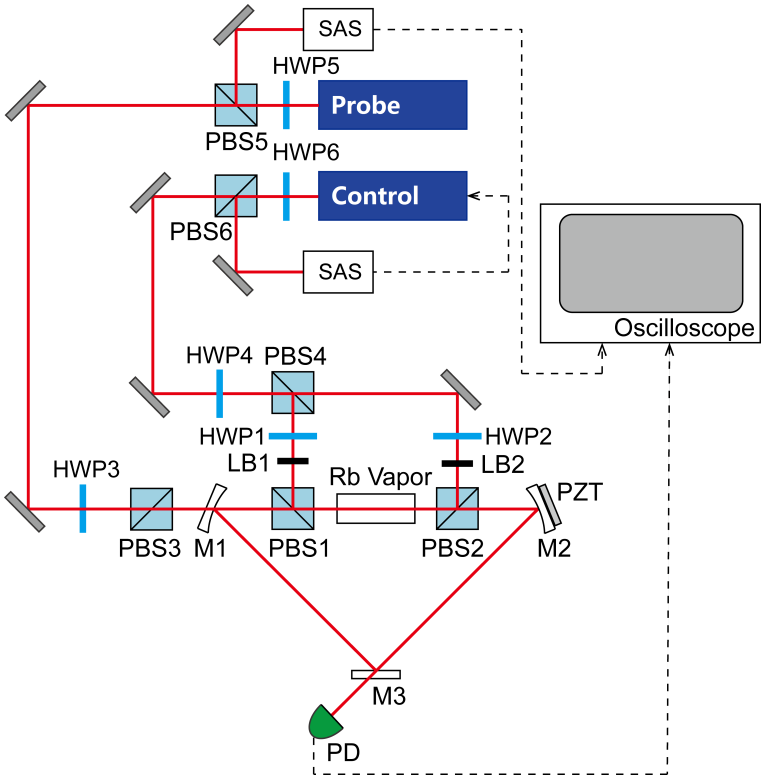

FIG. S3: **Detailed experimental setup.** Red lines represent optical paths, and black dashed lines represent electrical connections. PBS1-6 are polarizing cubic beam splitters; PD, photodiode dectector; M1-3 are cavity mirrors; PZT, piezoelectric transducer; HWP1-6 are half-wave plates.

long and is wrapped in μ metal. We use the three states of the ^{87}Rb D1 line, $5^2S_{1/2}, F = 1$ ($|1\rangle$), $5^2S_{1/2}, F = 2$ ($|2\rangle$) and $5^2P_{1/2}, F' = 2$ ($|3\rangle$). Two narrow linewidth (~ 1 MHz) tunable lasers with wavelength 795 nm are used as control and probe fields, respectively.

Part of the probe laser (~ 10 %) is split by PBS5 to a saturation absorption spectroscopy (SAS) setup to monitor the frequency of the probe field. In a similar manner, part of the control laser is split to the SAS to lock the frequency to be resonant with the atomic transition of $|2\rangle \leftrightarrow |3\rangle$. The probe laser power can be adjusted by half-wave plat (HWP3) and PBS3 to avoid the saturated absorption of the ^{87}Rb atoms and self-focusing effect. The probe laser, with a horizontal polarization, is injected into the cavity through the input mirror (M1) and is aligned to circulate inside the cavity as the cavity field. We use M3 as the output mirror, the output of the cavity is detected by a photodiode detector. The control laser, with a vertical polarization, is injected into the cavity and is separated by the PBS1,2. The control laser is carefully aligned to have a small angle with the probe laser to avoid circulating inside the cavity.

B. Detailed experimental setup for cold atoms

The experiment with cold atoms was done by trapping ^{87}Rb in a two-dimension magneto-optical trap (MOT). The MOT is obtained with 50 mW cooling laser supplying three perpendicular retro-reflected beams and 10 mW repump laser. The size of the cigar-shaped atom cloud about $2.5 \times 2.5 \times 10$ mm^3 and measured optical depth (OD) along axis is about 2. The temperature of cold atoms is about 200 µK. The experiment is run in a sequential mode with a repetition rate of 10 Hz. All lasers are tuned on or off by acousto-optic modulators (AOM) according to the time sequence described below. For each period of 100 ms, 99 ms is used for the cooling and trapping of the ^{87}Rb atoms, during which the cooling laser and the repump laser are turned on by two AOMs while the control laser and the probe laser are off. The time for the data collection lasts about 1 ms, during which the repump laser and the current to the anti-Helmholtz coils of the MOT are turned off first, and after a delay of about 0.1 ms, the cooling laser is turned off, and the control laser and the probe laser are turned on. After the control laser and probe laser are turned on by AOMs for 0.5 ms, the probe laser frequency is scanned across the ^{87}Rb D1 line, $5^2S_{1/2}, F = 1$ ($|1\rangle$), $5^2S_{1/2}, F = 1$ ($|2\rangle$) transitions, and the probe light transmitted through the cavity was then recorded versus the probe

frequency detuning.

C. Spectrum measurement

We measured the transmission of the probe field for co- and counter-propagation cases to demonstrate the non-reciprocal behavior of the system. In our experiment, changing the control laser direction is equivalent to changing the probe laser direction. To simplify the experimental setup, the control laser direction is reversed instead of reversing the probe laser. The propagation direction of the control laser beam can be switched to its opposite direction using HWP4 and PBS4. The control laser power can be tuned by adjusting the angle of the HWP1, 2. The laser blocking (LB) is used for blocking the residual control laser from the opposite direction and isolating the control laser from the SAS, which can induce unwanted noise. During the measurement, the control field is locked to the atomic transition of $|2\rangle \leftrightarrow |3\rangle$. The cavity mode is tuned to be resonant with the transition of $|1\rangle \leftrightarrow |3\rangle$ by tuning the voltage of the PZT. By scanning the probe field near the transition $|1\rangle \leftrightarrow |3\rangle$, the typical transmission spectrum is measured. In the experimental data processing, the transmission was normalized with the empty cavity transmission.

III. ADDITIONAL EXPERIMENT RESULTS

Though only the results for temperature at 55 °C are reported in the main text, we have actually performed a whole set of experiments at different temperatures ranging from 20 °C to 70 °C. The detailed results here will be useful to understand and design the optimal temperature for our ONR scheme under specific experimental conditions. In our experimental platform, Rb exits in vapor form in the cell. Thus, a change in temperature not only changes mean thermal motion velocities, but may also cause the number of atoms interacting with the cavity mode to change [5]. As such, a temperature change may also lead to a deviation from the collectively strong coupling condition, if there is a change in the number of atoms in the cavity.

Consider first how the transmission spectra change with temperature, as depicted in Figure S4b. It is seen that as the temperature increases from 20 °C to 70 °C, the transmission spectra evolve from a single-peak profile to a clear double-peak structure. In particular, only when the temperature is higher than 50 °C, can the vacuum Rabi splitting be identified from the experimental data in Fig. S4b. This is an interesting observation by itself, because it indicates that the CSCR condition in our current experimental platform starts to be met only when the temperature of the cavity hosting the warm Rb vapor is higher than 50 °C. Indeed, the observation in Fig. S4a supports this finding: there the system shows strong non-reciprocal only when the temperature is higher than about 50 °C. We have also estimated the change in the number of atoms as a function of the temperature by use of the temperature-dependence of the warm Rb vapor density. Our estimate shows that there can be indeed a significant change in the number of the atoms in the cavity in the concerned temperature range. However, the precise changes in the number of warm atoms are not important because it depends much on the details of our experimental setup.

Figure S4c depicts the normalized transmission versus temperature for co-propagation and counter-propagation cases. In both cases, the transmission decreases as the temperature increases. This echoes with, and can be explained by, the increase of the collective coupling strength as a result of temperature increase. For temperature at 55 °C, the counter-propagation transmission is almost zero, whereas the co-propagation transmission is still high. Solely for the purpose of achieving a high transmission contrast, one can certainly consider even higher temperatures. However, as seen from Fig. S4c, the transmission itself for the co-propagation case also decreases appreciably if the temperature is way above 55 °C. It is hence clear that there is an optimal temperature window, e.g., from 50 °C to 60 °C, in order to obtain both high transmission contrast and excellent transmission itself for the co-propagation case.

For parallel experiments for cold atoms, Fig. 4a in the main text indicated that we have reached the CSCR but observed almost perfectly reciprocal transmission. Here we present more results with a varying control field powers in Fig. S5. There the transmission increases from zero to 0.62 as the control field power increases from 0 mW to 6 mW. Remarkably, as depicted in Fig. S6, we always obtain that the transmission are virtually the same in co-propagation and counter-propagation cases, despite in the CSCR.

[1] Westgard, J. B. Introduction to Electrodynamics (Prentice-Hall, 1981).
[2] Iftiquar, S. M., Karve, G. R. & Natarajan, V. Subnatural linewidth for probe absortion in an electromagnetically-induced-transparency medium due to Doppler averaging. *Phys. Rev. A* **77**, 063807 (2008).
[3] Wang, Y.-H., Zhang, J.-P. & Zhu, Y.-F. Observation of dressed intracavity dark states. *Phys. Rev. A* **85**, 013814 (2012).

[4] Walls, D. F., and G. J. Milburn, Quantum Optics (Springer-Verlag, Berlin/Heidelberg, 1994).
[5] Steck, D. A. Rubidium 87 d line data, http://steck.us/alkalidata/ (2009).

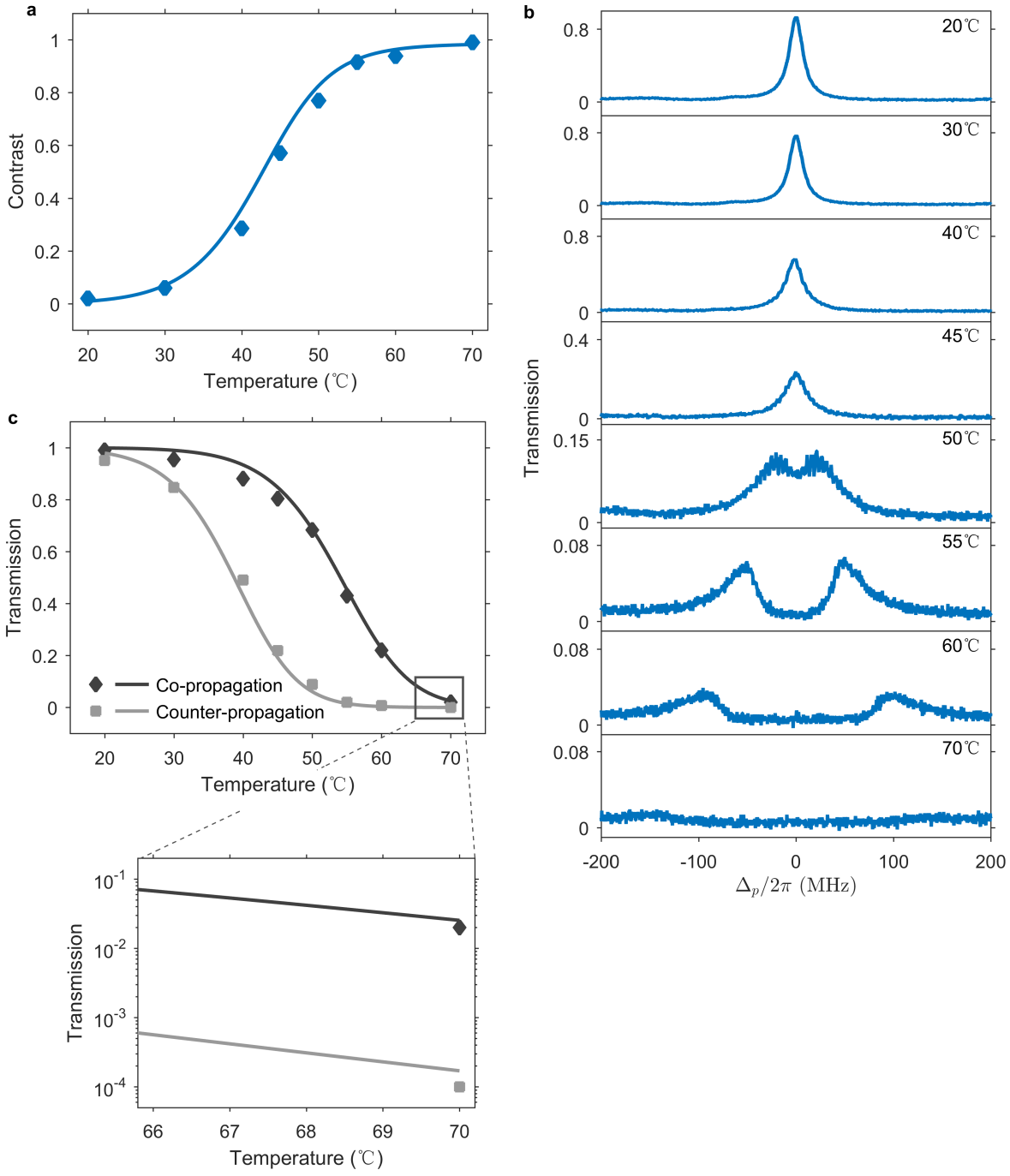

FIG. S4: **Experiment observation of non-reciprocal transmission with warm atoms a**, Transmission contrast vs temperature varying from 20 °C to 70 °C. The experimental probe field power is fixed at 12 μW and control field power is 12 mW. The dots are experimental results and curves are theoretical results. **b**, Normalized transmission spectra of the probe field without control field, exhibiting VRS when the temperature is higher than 50 °C. **c**, The co-propagation (black) and counter-propagation (gray) transmission vs temperature varying from 20 °C to 70 °C. The experiment parameters are same with **a**.

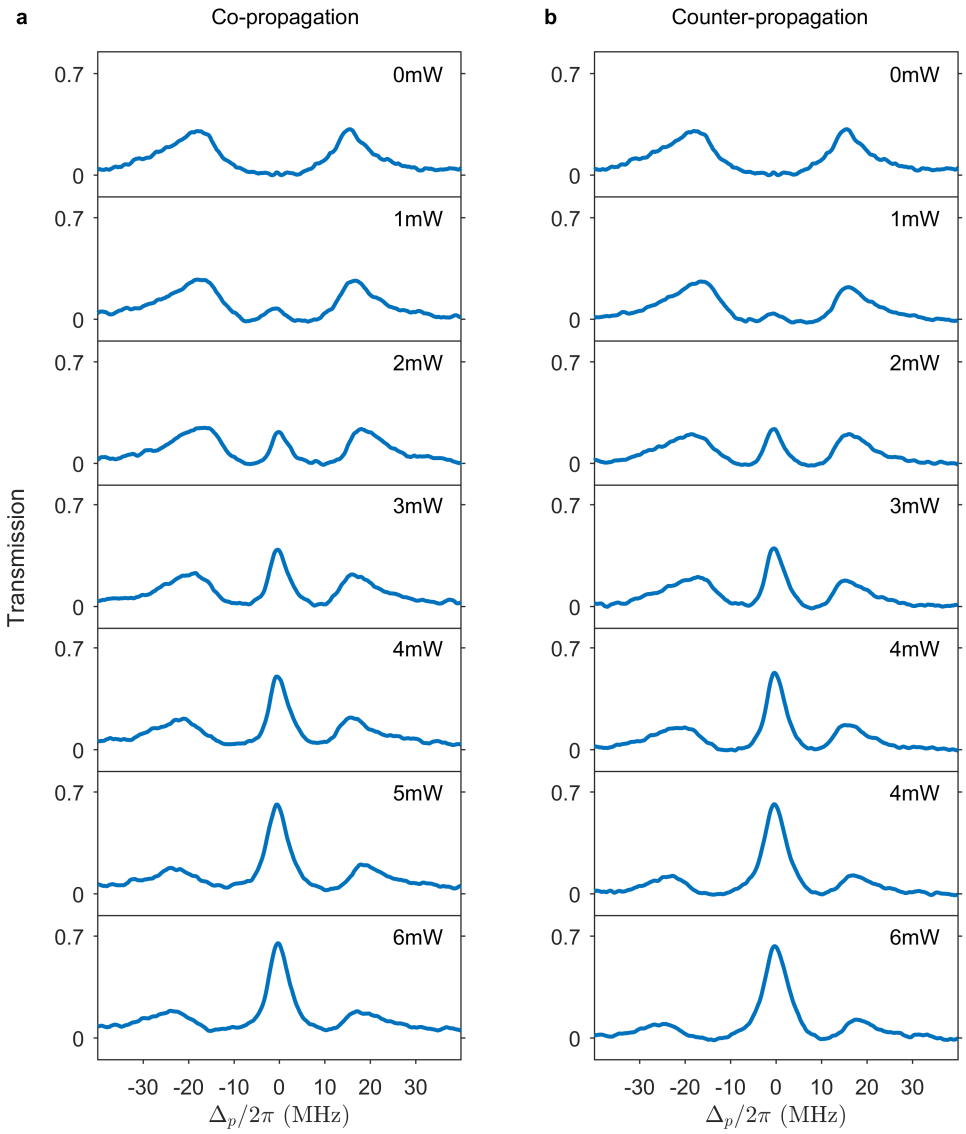

FIG. S5: **Experimental observation of reciprocal transmission with cold atoms. a**,**b**, Normalized transmission spectra of the probe field at different control field powers, $I_c = 0, 1, 2, 3, 4, 5, 6$ mW, for co-propagation (**a**) and counter-propagation (**b**) cases with a fixed probe field power $I_p = 0.5$ μW. The temperature of cold atoms is about 200 μK and optical density (OD) is about 2.

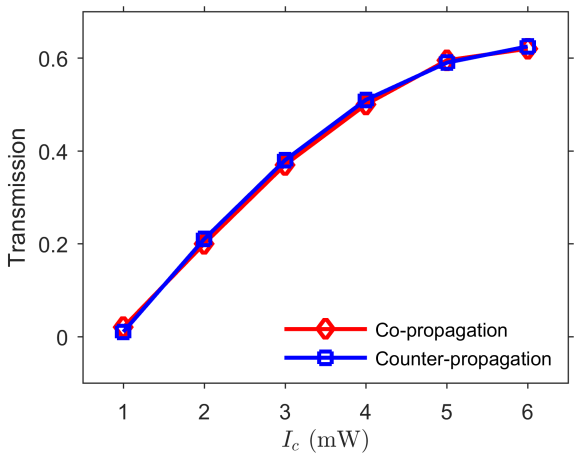

FIG. S6: **On-resonance transmission at different control field powers with cold atoms.** Normalized on-resonance transmission at different control field power for co-propagation (red) and counter-propagation (blue) cases with a fixed probe field power $I_p = 0.5$ μW.